Int. J. Electrochem. Sci., 8 **(2013)** 12692 - 12706

International Journal of ELECTROCHEMICAL SCIENCE
www.electrochemsci.org

Unsupported $Pt_xRu_yIr_z$ and Pt_xIr_y as Bi-functional Catalyst for Oxygen Reduction and Oxygen Evolution Reactions in Acid Media, for Unitized Regenerative Fuel Cell

L. Morales S[1]*. and A.M. Fernández*[2,*]

[1]Posgrado en Ingeniería, Energía UNAM
[2]Departamento de Materiales Solares, Instituto de Energías Renovables, Universidad Nacional Autónoma de México. Privada Xochicalco s/n, Temixco, Morelos, 62580, México. Tel/fax directo 5622-9742 ext 29705
[*]E-mail: afm@ier.unam.mx

Received: 6 June 2013 / *Accepted:* 21 August 2013 / *Published:* 20 October 2013

The effect of Ru on the activity of unsupported $Pt_xRu_yIr_z$ material was analyzed in 0.5 M H_2SO_4 for $O_2+4H^++4e^- \leftrightarrows H_2O$ reaction. Pt_xIr_z, $Pt_xRu_yIr_z$ Pt, Ir and Ru materials were prepared by chemical reduction. The electrocatalytic activity was evaluated by Linear Sweep Voltammetry, Rotating Disk Electrode and Cyclic Voltammetry. $Pt_xRu_yIr_z$ showed an improvement to ORR after potential for interest reaction was applied. Ruthenium electrochemical activity disappears when to subject to anodic potential. Catalytic materials had particle sizes of 5-10 nm. $Pt_xRu_yIr_z$ alloy formation phases were observed by High Resolution Transmission Electron Microscopy. No evident electrochemical changes were observed to Pt_xIr_z material at ORR.

Keywords: Unitized Regenerative Fuel Cell (URFC), Electrocatalysts, Bifunctional oxygen electrode, Fuel Cell, Water Oxidation Reaction and Oxygen Reduction Reaction.

1. INTRODUCTION

Unitized Regenerative Fuel Cell (URFC) is an electrochemical cell that works as polymer electrolyte fuel cell and a polymer electrolyte water electrolyzer into the same unit. URFC system has been developed for different energy management systems, including High-Altitude Long Endurance (HALE) aircraft, Solar Rechargeable Aircraft (SRA), Zero Emission Vehicles (ZEVs), hybrid energy storage/propulsion system for spacecraft and energy storage for remote (off-grid) power sources [1-2]. The structure and composition of electrocatalytic layers in URFC´s are of particular importance and strongly impact current–voltage performances and cell efficiencies. In comparison to conventional

H_2/O_2 fuel cells and water electrolyzer, the structure of electrocatalytic layers for URFC is even more complicated due to the specific requirement of bi-functionality [3]; electrocatalytic layer in a URFC must perform the reversibility of reactions, however the perform is limited by electrocatalytic materials.

Some electrocatalyst materials used for Oxygen Reduction Reaction (ORR) have demonstrated low activity for Oxygen Evolution Reaction (OER). Contrary some of them apply for OER have poor ORR performance. The ORR and OER are carried out in the same electrode (Oxygen electrode) in an URFC [3-8]. In order to facilities the nomenclature, Oxygen electrode and Hydrogen electrode terms are used to refer as electrodes in URFC. Different electrocatalytic materials have been proposed for oxygen electrode, for example mixing Pt black, as electrocatalysts for oxygen reduction, and Ir or IrO_2-RuO_2 as electrocatalysts for oxygen evolution [4-8]. The formation one or two layers of electrocatalyst materials on membrane were realized to build the oxygen electrode in a URFC [8].

In order to improve the dispersion of a bifunctional electrocatalytic material onto the membrane, different techniques of synthesizes were developed [3,6,10-11], an also various atomic composition electrocatalysts [12-15].

Chen *et al*. [10] identified that the ternary electrocatalysts $Pt_{4.5}Ru_4Ir_{0.5}$ (subscripts indicate atomic ratios) is the most efficient and stable electrocatalyst for the Oxygen electrode in a URFC system after to combine five elements (Pt, Ru, Os, Rh and Ir) using combinatorial technique. He also showed that the addition of Ru in the Pt-Ir electrode increase the reaction rate by stabilizing the surface atom/oxygen bonds [16]. Pt-Ru-Ir supported in Carbon black and Vulcan has been used for electro oxidation of methanol system [17-18].

Pt_xIr_z and $Pt_xRu_yIr_z$ materials were synthetized by chemical reduction. Physical and electrochemical characterization as bi-functional electrocatalytic material for $O_2+4H^++4e^- \leftrightarrows H_2O$ reaction were analyzed in this paper. Pt, Ru and Ir material were evaluated in order to compare with Pt_xIr_z and $Pt_xRu_yIr_z$.

2. EXPERIMENTAL DETAILS

2.1 Preparation of unsupported electrocatalysts

Unsupported $Pt_xRu_yIr_z$ electrocatalysts was prepared with 3.88 mM of Hexachloroplatinic acid (H_2PtCl_6 *H_2O Fluka purum, 38% Pt), 4.4 mM of Ruthenium (III) Chloride ($RuCl_3$*H_2O reagent plus Sigma-Aldrich) and 1.66 mM of Iridium (III) Bromide ($IrBr_3$*H_2O Sigma-Aldrich). It were dissolved in deionizer water (Millipore 18MΩ), in order to prepare an aqueous solution. 5% of molar excess of aqueous Sodium Borohydride ($NaBH_4$, reagent grade ≥98.5% Sigma-Aldrich) was added to the aqueous solution. After 20 minutes, it was obtained a precipitate. The suspension was filtered, washed and treated at 200°C during 2 hr in N_2 flux, to remove all Oxygen content. Other materials as Pt_xIr_z, Pt, Ir and Ru were also synthesized with the same procedure.

2.2 Physical characterizations

The X-Ray Diffraction (XRD) pattern was recorded using a Rigaku DMAX-2200 diffractometer with CuKα (λ = 1.5418 Å) radiation source operating at 36 kV and 30 mA. The XRD samples were carried out in the angle (2θ) range from 10° to 100° at a scan rate of 0.0066 °/s. Silicon powder (typically 1-20 μm, 99.9985% purity, Alfa Aesar) was used as an internal standard. Joint Committee on Power Diffraction (JCPDS) cards were used in order to compare the phases and a crystalline structure obtained by XRD technique. Software Jade 6.5 was used to estimate the average crystal size of samples.

The morphology of synthesis materials was observed using the FESEM-Hitachi S-5500 High Resolution Scanning Electron Microscopy (HRSEM) with accelerating voltage of 10KV. The phase distinction was examined by equipment JEOL JSM-7600T microscopy. The chemical composition of electrocatalytic materials was obtained by using Energy Disperses Spectroscopy (EDS) equipment installed in the same microscope. In addition, Transmission Electron Microscopy (TEM) images were taken using a JEOL JEM 1200EX microscope operating at 120KV. The microphotographs were filtered with Digital Micrograph ™ software version 3.7.0. The samples were prepared by dispersing the electrocatalytic material onto a carbon-coated copper grid in order to analyze by TEM. Analysis by High Resolution Transmission Electron Microscopy (HRTEM) was using a JEOL 2010FEG FASTEM with a resolution of 1.9Å.

2.3 Electrochemical evaluation of electrocatalysts

A quantity of 3 mg of unsupported powder and 15 μl of Nafion® solution (5 wt. % Aldrich) were dispersed into 300 μl of deionizer water (18.2 $M\Omega.cm^2$) and sonicated for at least 30 minutes in order to make an electrocatalyts ink. A micropipette was used to deposit the ink (0.185mg) onto glassy carbon coated with Teflon and dried at room temperature to build the Working Electrode (WE).

The WE was evaluated in a three-electrode cell containing a Pt mesh Counter Electrode (CE), an Ag/AgCl/KCl as Reference Electrode (REF, offset potential vs. Normal Hydrogen Electrode: 0.197 V), and the 7 mm diameter glassy carbon, covered with the electrocatalyst deposit. The cell solution was 0.5 M H_2SO_4 purged with N_2 (Infra Co; Ultra High Purity UHP, 99.999% MIN) or O_2 (Infra Co; zero grade, UHP). Electrochemical techniques as Cyclic Voltammetry (CV), Linear Sweep Voltammetry (LSV) and Rotating Disk Electrode (RDE) were carried out using Potentiostat/Galvanostat equipment (VSP-Biologic).

All electrocatalyst were first electrochemically cleaned by cycle scanning from -0.2 V to 0.8 V at $10mVs^{-1}$ for 30 cycles, followed by CV scanning from 0.8 V to 1.4 V and then back to 0.8 V by step of 0.1V in N_2-saturated aqueous solution. The interest range work potential was conclude on basis previous analyses. LSV technique was performed from Open Circuit Potential (OCP) to 0 V for ORR in O_2 saturated aqueous solution and then from 0.8 V to 1.4 V for OER in N_2 atmosphere at scan speed of $5mVs^{-1}$. This sequence was repeated twice.

The kinetic parameters were estimated with RDE technique for ORR using a Pine Analytical rotator (EG&G PARC model 616). Two experimental conditions were used to evaluate those

parameters. Condition 1 began with the ORR at different rpm in O_2-saturated atmosphere (OCP to 0 V), followed by cycle scanning from OCP to 1.4 V by step of 0.1V for OER. Condition 2 was opposite to Condition 1. After OER conclude in each experimental condition, it was realized an electrochemical cleaning.

Two different potential ranges were applied to measurement the stability of WE, the first one was from -0.2 V to 0.8 V and the second one from 0.8 V to 1.4 V, these corresponds for ORR and OER respectively. It was applied 300 cycles at scan rate of $10mVs^{-1}$. All electrochemical evaluation data were collected using EC-Lab V10.23 and all results obtained were plotted versus Normal Hydrogen Electrode (NHE).

3. RESULTS AND DISCUSSION

3.1 Physical characterization and analysis

Figure 1 shows the XRD partner of Pt_xIr_y and $Pt_xRu_yIr_z$ synthesized by chemical reduction technique and Pt-Ru-Ir mixture also synthesized each by chemical reduction. It was found that the diffraction peaks correspond to (111), (200), (220), (311) and (222) plans for the sample $Pt_xRu_yIr_z$ that coincide with the peaks of PtIr (JCPDS 01-071-9289). Apparently there is no presence of Ru or its oxide form, in the ternary compound. Jingpeng Wang *et. al* [19,20] report that the presence of Ru provoke the increase in the diffraction angle for Pt-Ir and Pt-Ru alloys due that the lattice parameter reduce. Sivakumar Pasupathi *et.al* [21] found that Pt-Ru-Ir synthesis by vapor deposition technique; the XRD peaks for Pt and Ir were displaced.

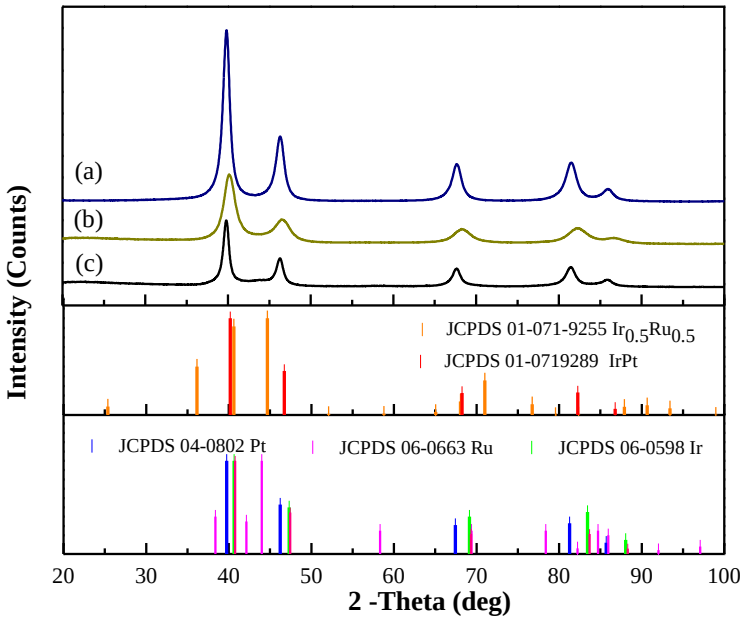

Figure 1. Powder diffraction patterns of (a) Pt_xIr_z, (b) $Pt_xRu_yIr_z$ and (c) mixtures of Pt, Ru, Ir in the same composition of Pt-Ru-Ir material synthetized by chemical reduction.

Yongmin Liang *et. al*.[22] using the MIPA technique prepared PtRuIr/C and PtRu/C electrode and they found in all cases the XRD peaks were close to Pt phase without any trace of Ru [23,24]. Bo Yang *et. al.* [23] prepared PtRu/C using the Antolini *et.al.* [25,26] methodology and they found that small percentage of Ru was crystalline in the Pt-Ru alloy, and the rest was amorphous. By XPS analysis Xin Zhang *et.al*.[27] found that the Pt-Ru alloy was a solid solution with a Pt^0, Ru^0, Ru^{+4}, RuO_2, Ru^{+6} and RuO_3.

According with the Figure 1(a) Pt_xIr_z had similar XRD pattern of Pt (JCPDS 04-0802). By XRD analysis of Figure 1(b), the interplanar distance value for $Pt_xRu_yIr_z$ was less that Pt, this observation it was reported before by Wang *et. al.*[19]. This reduction was attributed to the Ru incorporation, as A.S. Aricó *et al*. [28] previous report, and also cause a reduction in the crystal size, that in this case for $Pt_xRu_yIr_z$ that was 9 nm, meanwhile for Pt was 14nm. From the same Figure 1 it can see that the XRD peaks of Pt-Ru-Ir mixture (Figure 1(c)) coincide with Pt (JCPDS 04-0802), it was attributed to the major content of Pt in this mixture.

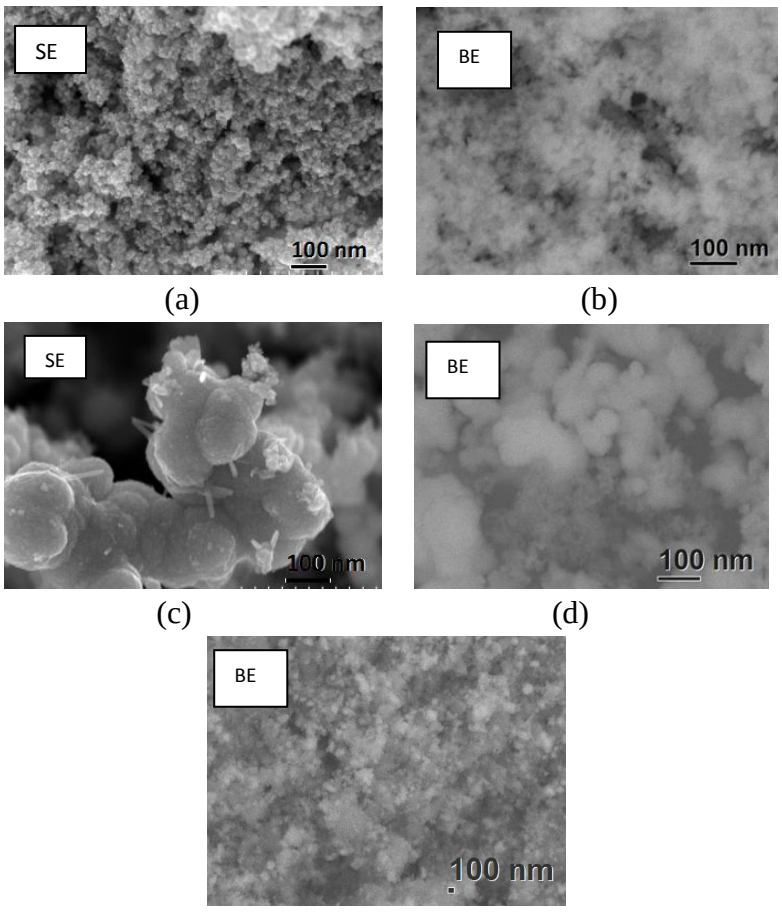

Figure 2. SEM images by secondary (SE) and backscattering (BE) electrons of (a), (b) Pt_xIr_z,(c),(d), $Pt_xRu_yIr_z$ and (e) BE mixture of Pt, Ru, Ir

The microphotographs of Secondary (SE) and Backscattering (BE) electrons for Pt_xIr_z and $Pt_xRu_yIr_z$ catalyst are shown in Figure 2. It is an important to mention that with images can distinguish the elements using the intensity of gray color scale, the elements with dark gray color has low atomic

number and backwards. For example in Figure 2(b) it observed a major clear gray color regions that it is an indication of the presence Pt and Ir, which they have close atomic value. The microstructure of Pt_xIr_z catalyst material is dense (Figure 2(a)). In Figure 2(c) is possible to see a formation of sphere forms with small nanorods. Figure 2(d) and (e) show the morphology of $Pt_xRu_yIr_z$ electrocatalyst made by chemical reduction and a mixture of Pt-Ru-Ir respectively. It can note that for $Pt_xRu_yIr_z$ has a sphere formation and agglomerate, and according with the gray intensity color, it can distinguish two intensity gray color, one more clear and other more dark, the first probably correspond to presence of Ir and Pt and the dark part to Ru. However, in the case of the mixture it can see different intensities gray colors; it is due to the formation of mixture of the three elements. EDS analysis values coincide with the suggested ratio of the synthesis: it is expected a high content of Platinum, Ruthenium and poor Iridium (Table 1).

Table 1. Atomic and weight percentage composition of electrocatalytic materials synthesis by chemical reduction, obtained by EDS

	Pt_xIr_z		$Pt_xRu_yIr_z$	
Element	Weight%	Atomic%	Weight%	Atomic%
Ru L	-	-	29,57	38,92
Ir M	5,495	18,8375	4,9	17,17
Pt M	94,505	81,1625	65,54	43,9
Total	100	100	100	100

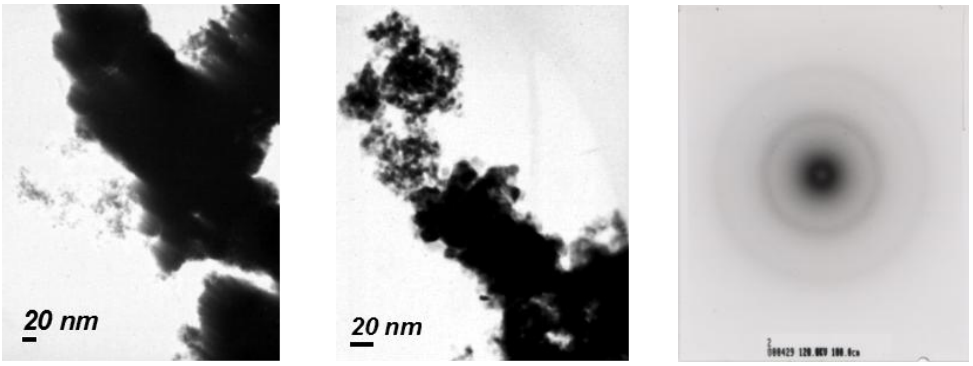

(a) (b) (c)

Figure 3. Bright field of TEM images of $Pt_xRu_yIr_z$ (a) 150KX, (b) 250KX and (c) Diffraction pattern at 120KV with 150KX

Figure 3(a) and (b) shows TEM images in bright field of the $Pt_xRu_yIr_z$, after processing with a Digital Micrograph ™ software version 3.7.0, and it is possible to note the formation of two zones, one with agglomerated particles and other segregate particles. This type of formation was also observed by Eguiluz KIB *et.al.* [29] who synthesized different composition of $Pt_x(Ru\text{-}Ir)_y/C$ prepared by sol-gel technique and found similar zones, and after EDS analysis meet small particles of Pt and the agglomerated close to 10 nm that correspond to Ir and Ru. Diffraction pattern of the TEM images of

$Pt_xRu_yIr_z$ is in Figure 3(c), from this figure it can see diffuse rings pattern at different directions which is an indication that the electrocatalyst material has not adequate crystallinity, however the interplanar distance in this figure is more close to $Ir_{0,6}Ru_{0,4}$ [JCPDS 03-065-5546] with (111) (200) (220) and (420) planes and also it was found the phase of Ru [JCPDS 06-0663] with (100) plane.

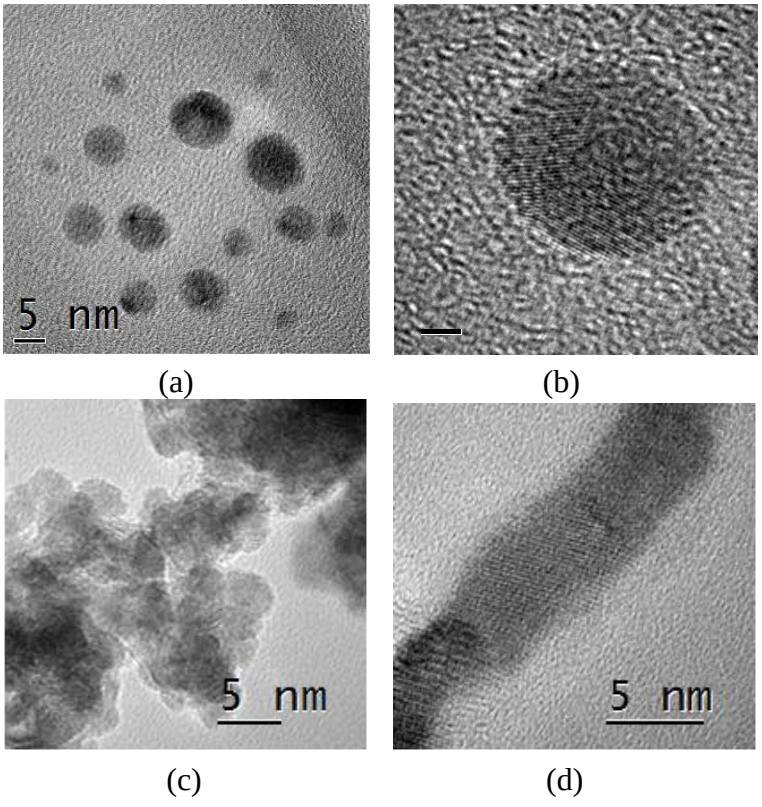

Figure 4. HRTEM microphotographs of $Pt_xRu_yIr_z$ electrocatalyst material prepare by chemical reduction, (a) 400KX, (b) a macle formation to1,300 KX, (c) 860KX, (d) 130 KX, nanorod

The particle size of $Pt_xRu_yIr_z$ was 3 to 10 nm according with the Figure 4(a), where also it observes a macle formation [30] (Figure 4(b)). After the analysis of these images using the Figure 4(c), it was determinate the formation of two phases that correspond to IrRu [JCPDS 01-071-9300] and $Ir_{0.44}Ru_{0.56}$ [JCPDS 03-065-5982]. As it showed previously in Figure 2(c) a nanorod formation, and in Figure 4(d) shows a resolution image of presences these nanorods. Liu, f. *et al*.[31] found a similar formation of nanorodes with 200 nm of diameter during a synthesis of Pt-Ru tandems by electrodeposition technique, also J. Chen *et.al.* [32-34] synthesized Pt nanowires with 5 nm of diameter.

3.2 Electrochemical characterization

A similar electrochemical behavior was observed between Pt_xIr_z and Pt electrodes as it shows the voltamperogramms of Figure 5(a).

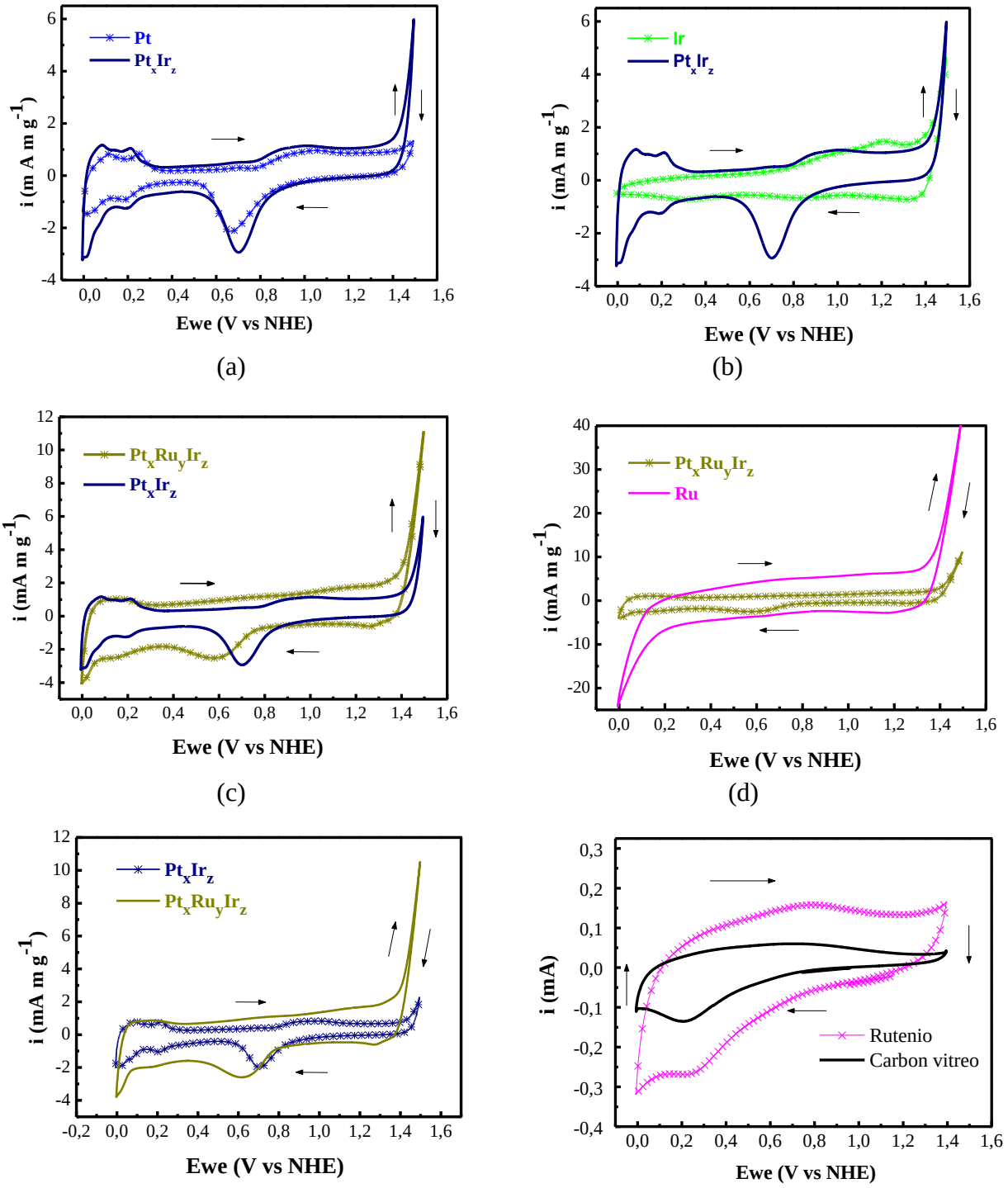

Figure 5. Cyclic voltamperograms in 0.5 M H_2SO_4 aqueous solution, scanning rate at 10mVs^{-1} from OCP to 1.4V by step of 0.1V for (a) Pt_xIr_z and Pt, (b) Pt_xIr_z and Ir, (c) $Pt_xRu_yIr_z$ and Pt_xIr_z, (d) $Pt_xRu_yIr_z$ and Ru. Cyclic vomtamperogram after at 1.4V was applied. (e) $Pt_xRu_yIr_z$ and Pt_xIr_z, (f) Ruthenium and glassy carbon.

An increment in the current is evident before 1.4 V in anodic regions and after 0.9 V in cathodic region for comparison Pt_xIr_z to Pt electrode due to content of Iridium (Figure 5(b)). There are some reports [35,36] where mention that combine Pt with Ru or RuO_2 and Ir or IrO_2 is adequate for

ORR. $Pt_xRu_yIr_z$ electrode did not showed Hydrogen adsorption/desorption peaks. Also, a displacement of potential to less positive values and an increment of the current after 1.3 V were observed (Figure 5(c)), it is possible due to the Ruthenium presence.

After OER was done at WE, it was observed some electrochemical changes. The potential of ORR at $Pt_xRu_yIr_z$ electrode was similar to Pt_xIr_z electrode and the intensity of current for OER was decreased in Pt_xIr_z electrode (Figure 5(e)). Instable electrochemical activity at Ruthenium electrode is shows in Figure 5(f). From the same figure it can note identical behavior with glassy carbon as if Ruthenium was not on surface of glassy carbon. If it compares Ruthenium voltamperogram (Figure 5(f)) versus Figure 5(d), it found they are very different; as a consequence there is not activity of Ruthenium. Some reports [37, 38] also mention that the no activity for Ru is due to formation of RuO_4 who is a non-conductive material. Reier T. *et.al.*[39] used ICP-OES (Inductively Coupled Plasma Optical Emission Spectrometry) technique in order to analyzed the amount Ru in the solution after OER, they found that after applied a scanning voltage some amounts of Ru, that they assumed the formation of RuO_4, and they confirmed with *in-situ* Reflectance technique [38].

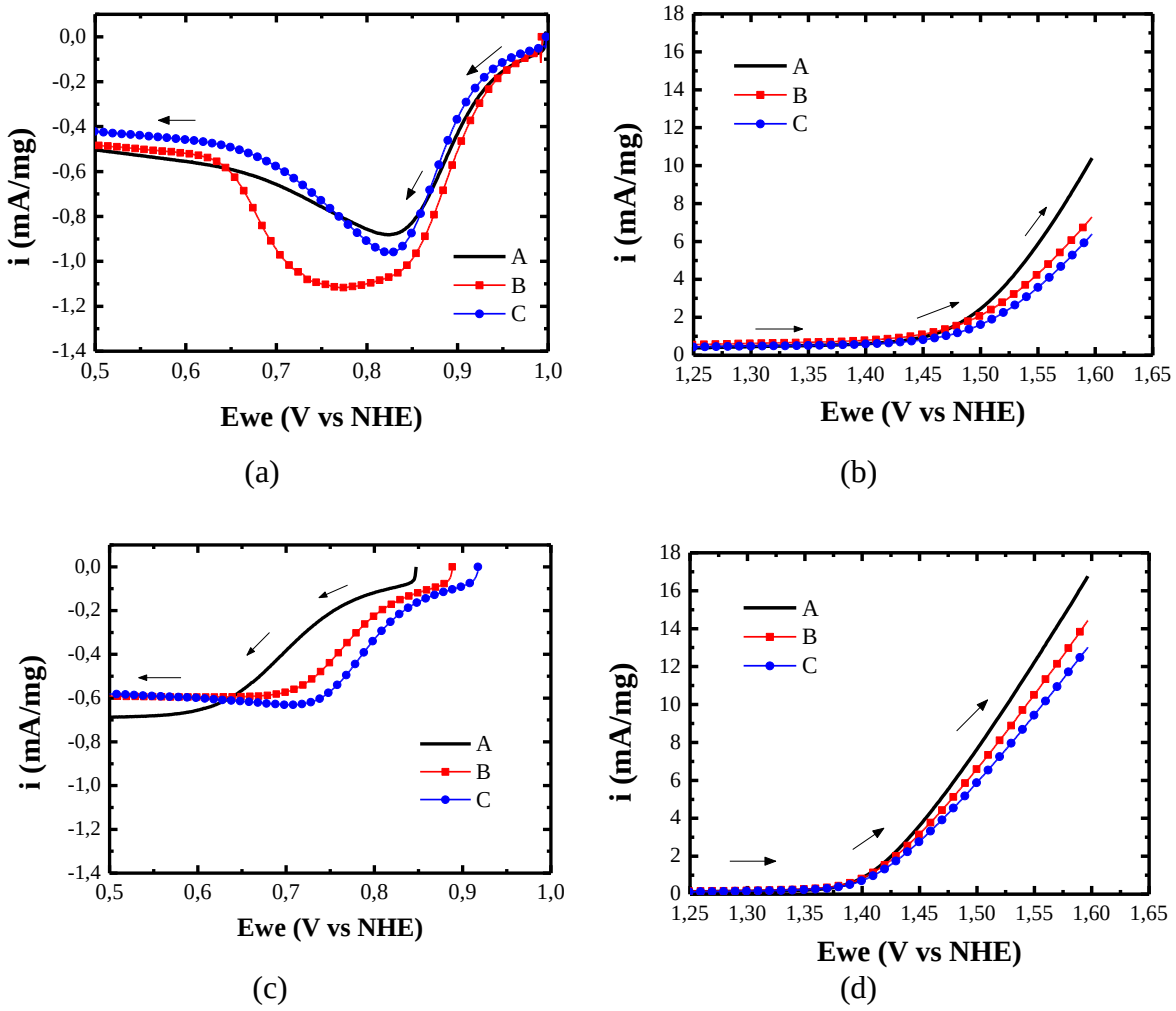

Figure 6. Linear Sweep Voltamperometry (LSV) for Oxygen Reduction and Oxygen Evolution Reaction for (a),(b) Pt_xIr_z and (c),(d) $Pt_xRu_yIr_z$ catalyst material

Binary and ternary materials were evaluated with LSV technique as it shows in Figure 6. A sequence of performer was subjected at WE to verified changes when switching from ORR to OER respectively. In $Pt_xRu_yIr_z$ was encountered an increment in startup potential for ORR after to realized the OER (Figure 6(c)). That means that ORR was benefited. On the other hand in the sequence of repetition at same electrode, Pt_xIr_z was a notable decrease of current in OER (Figure 6(b)). $Pt_xRu_yIr_z$ decreased too but in smaller proportion (Figure 6(d)). Ternary material had a better electrochemical activity for OER and Pt_xIr_z for ORR (Figure 6(a)).

Data of curves of polarization for ORR at different speed rotation were analyzed. Three zones of total current were recognized. Polarization curves of $Pt_xRu_yIr_z$ electrode are showed in Figure 7(a); it was recognized the process by the charge transfer between 0.9 V and 0.8 V. There was not current variation with respect to the different rotation speed.

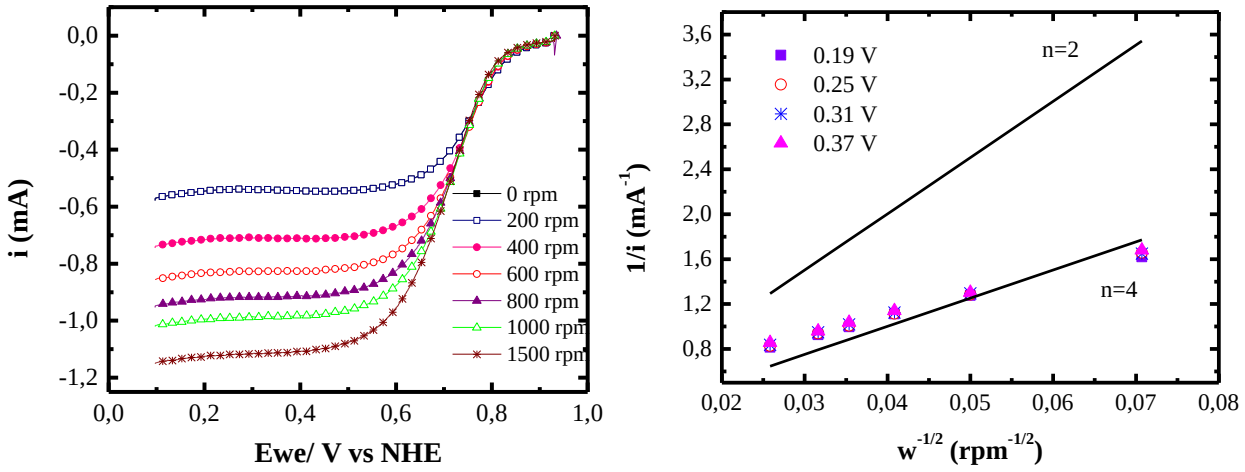

(a) (b)

Figure 7. Oxygen reduction polarization curves obtained on the $Pt_xRu_yIr_z$ catalyst at different rotation speeds, and (b) Koutecky–Levich plots obtained for the $Pt_xRu_yIr_z$ catalyst at 0.37, 0.31, 0.25 and 0.19 V (vs. NHE).

Also, according with the Figure 7(a), the mixed control zone was determinate in the range of 0.8 V to 0.5V. The third zone in the figure was found between 0.5V to 0.2 V; it is defined as transport-limited current. The analysis [40,41] of third zone was made using the Koutecky–Levich relation, which this zone is dependent-function of the angular velocity. The total current (i) is related to the rotation speed by Koutecky–Levich relation:

$$(1/i) = (1/i_k) + (1/Bw^{1/2}) \quad (1)$$

where i_k is the kinetic current, B is the Levich slope and w is the rotation speed of RDE. The Koutecky–Levich slope is given by:

$$B = (0.2)nFcD^{2/3}v^{-1/6} \quad (2)$$

where n is the number of electrons transferees per O_2 molecule, F is Faraday constant, c is the concentration of O_2 in the solution (1.1exp(-6) molcm^{-3}), D is the diffusion coefficient of O_2 in the solution (1.5 exp(-5) cm^{2}s^{-1}), and ν represents the kinetic viscosity of the solution (1exp(-2) cm^{2}s^{-1}).

The 0.2 value is a constant and it used when w is expressed in revolutions per minute. Different potentials were selected at diffusion limited current zone. In the Figure 7(b) shows the Koutecky–Levich slope estimated of experimental and theoretical data, for n = 2 and n = 4 at $Pt_xRu_yIr_z$ electrode. It was observed that experimental slope is close to n = 4, it means that electrocatalyst is carried out by four electrons reduction path for the geometric area of 0.385 cm^2. It was estimated alike one for Pt_xIr_z. Electro active area for electrocatalysts was analyzed by RDE with the relation of B theory and B experimental (Table 2).

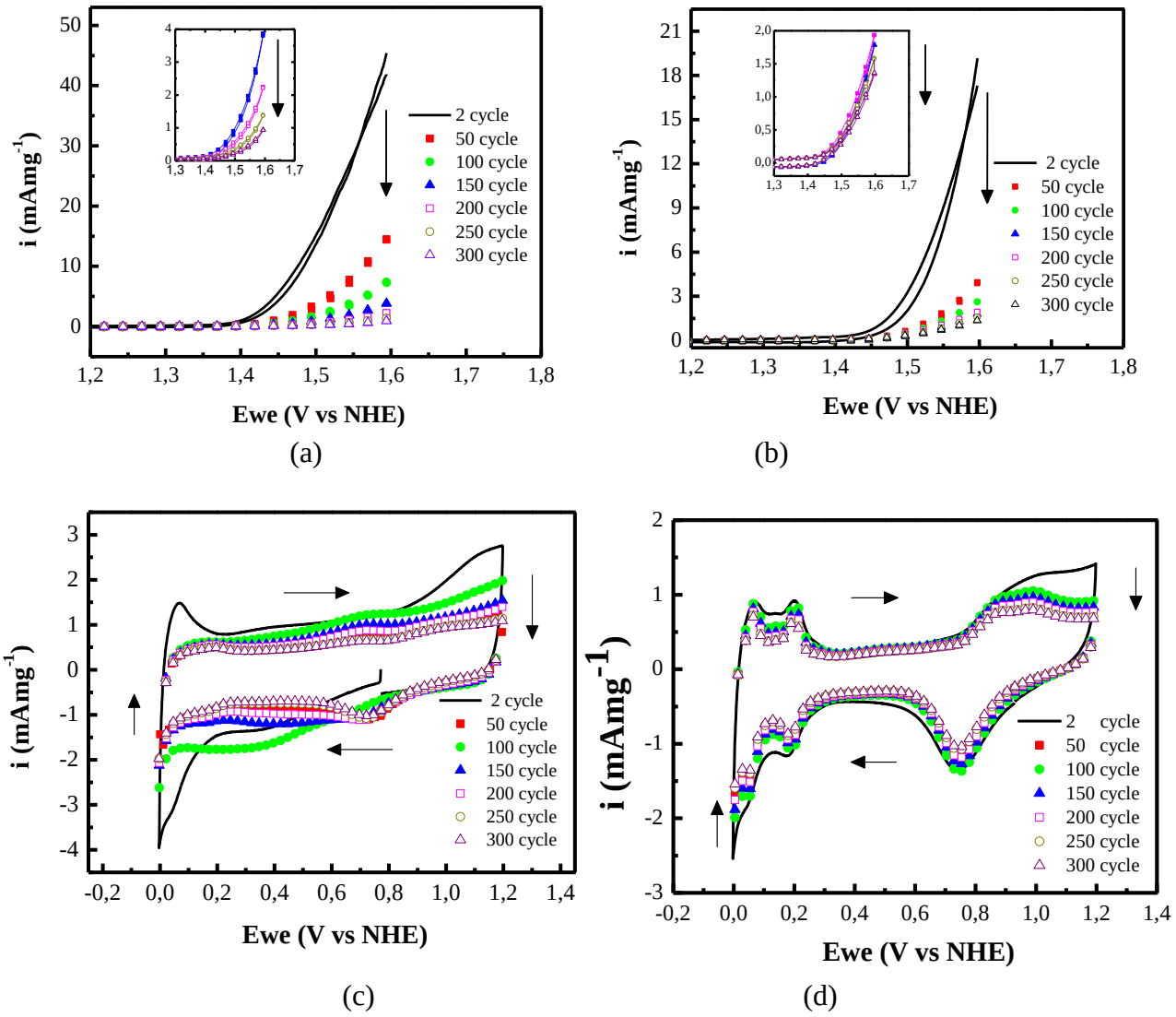

Figure 8. Cyclic voltamperograms for Oxygen Evolution Reaction on (a) $Pt_xRu_yIr_z$ and (b) Pt_xIr_z electrode and for Oxygen Reduction Reaction on (c) $Pt_xRu_yIr_z$ and (d) Pt_xIr_z catalysts in 0.5M H_2SO_4 aqueous solution, scanning rate at 10mVs^{-1}

Figure 8 shows the variation of current for ORR and OER at 300 cycles in electrocatalyts electrode. In Figure 8(a) and (b) it was observed instability of $Pt_xRu_yIr_z$ and Pt_xIr_z electrode. $Pt_xRu_yIr_z$ had a current increment of 45mA mg^{-1} and second cycle start to decrease until 0.8 mA mg^{-1} at 300 cycle. In Pt-Ir electrode had 20mA mg^{-1} which decrease until 1.36 mA mg^{-1}. During the last four cycles (300,250,200 and 150 cycle) Pt-Ir electrode had not variation in current, however for Pt-Ru-Ir, the current variation reduce with small increment.

Figure 8(c) and (d) shows ORR cycles on $Pt_xRu_yIr_z$ and Pt_xIr_z electrodes respectively. According with these results Pt_xIr_z had not variation in potentials reaction (Figure 8(d)), however for Pt-Ru-Ir electrode, after 50 cycles had a variation, as it can see in Figure 8(c).

Kinetic parameters, such as transfer coefficient (α), Tafel plot (b) and current exchange (i_0) were determinate by corrections of the total current due to the mass transfer contribution in the Tafel plot by using the following equation:

$$i_k = (i_{exp} \text{ x } i_{lim}/(i_{lim} - i_{exp}) \quad (3)$$

where i_{exp} represents experimental data and $i_{lim}=Bw^{1/2}$ calculated by Koutecky–Levich with B experimental data.

Table 2. Kinetic parameters for ORR of Pt_xIr_z and $Pt_xRu_yIr_z$ catalysts in 0.5M H_2SO_4 solution. Condition 1 and 2 are described in Experimental Section.

Catalyst material	Experimental		Electroactive area	bc	α	i_0
			m^2/gr	mV/dec	-	mA
$Pt_xRu_yIr_z$	Condition 1	A	0.282	-162	0.4	9.31E-05
		B	0.247	-179	0.36	3.61E-04
	Condition 2	C	0.274	-151	0.43	1.89E-04
Pt_xIr_z	Condition 1	A	0.252	-83	0.8	3.89E-06
		B	0.235	-82	0.8	1.88E-06
	Condition 2	C	0.223	-96	0.6	1.38E-05

Figure 9 shows Tafel correction plot for $Pt_xRu_yIr_z$ and Pt_xIr_z electrode according to experimental conditions. The polarization curve designed as A, it is the electrocatalytic material without being subjected to the OER; B represents the same electrode but has been subjected to OER. Finally, C correspond another experimental condition; in this electrode was subjected first to OER and then it was made RDE analysis for ORR. Different Tafel plots were encountered after to scan until 1.6 V vs NHE (Figure 9 (c) and (d)).

Startup potential for ORR was improved in B and C polarization curves for $Pt_xRu_yIr_z$ electrocatalyst material. Also, it was observed that current is controlled by diffusion; it is recognizing by slope type at the beginning of polarization potential (Figure 9(a)). At Pt_xIr_z electrode did not shown significant changes in its polarization curves.

Tafel plots values for ORR are close to 60 $mVdec^{-1}$ for Pt at low overpotential, however values around 120 $mVdec^{-1}$ are for metals as Ru and Pd [42-44]. According with our calculation $Pt_xRu_yIr_z$ had Tafel plots values relative higher than suggest by literature. Under Condition 1 (Table 2) the difference of Tafel values between A and B is 17 mV, which is a significant after ORR, and the current exchange was reduced after applied high potential, according with B curve, however for Pt_xIr_z the ORR was better and the i_o is higher in comparison with $Pt_xRu_yIr_z$, as it shows in Table 2. Current exchange was normalized in ratio with electro active area.

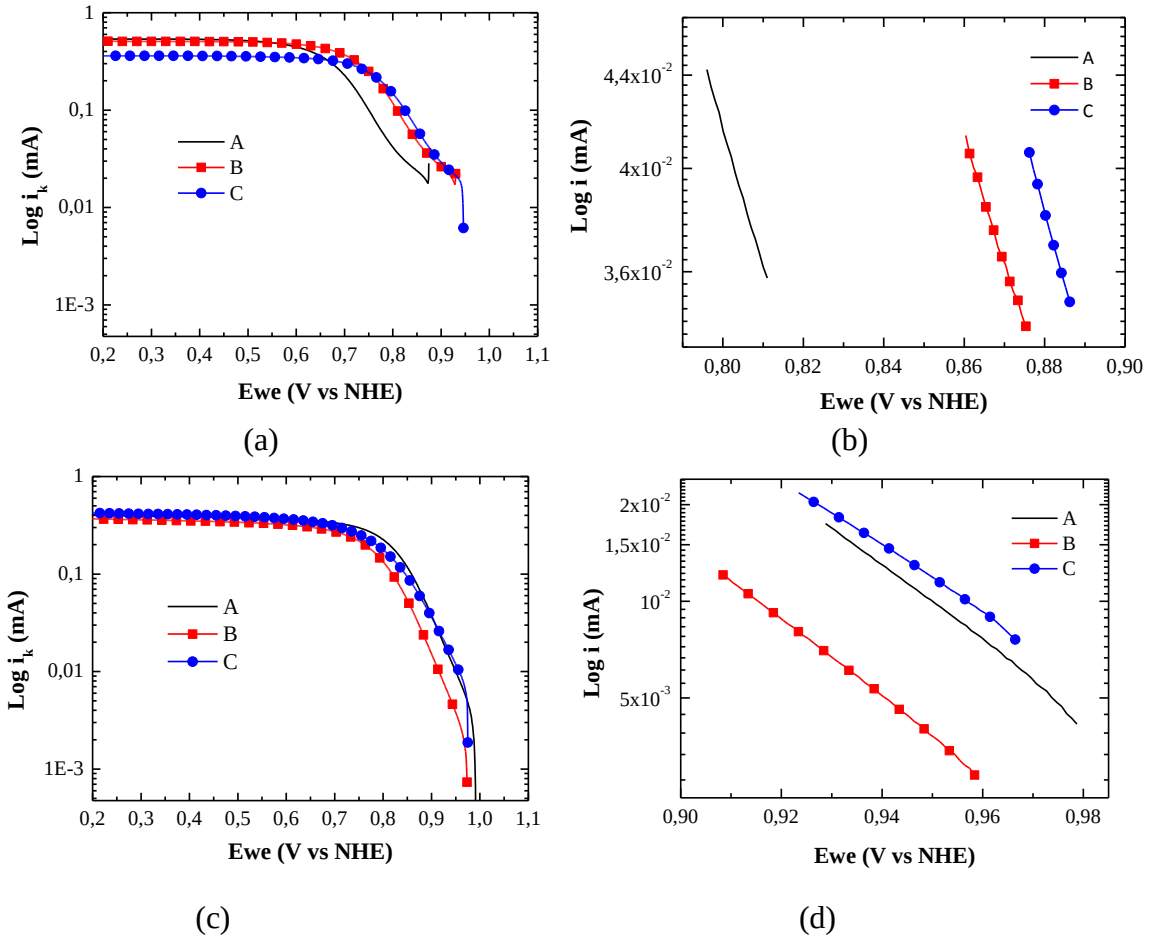

Figure 9. Tafel plots correction for ORR on (a),(b) $Pt_xRu_yIr_z$ and (c),(d) Pt_xIr_z in 0.5M H_2SO_4 at 5mVs^{-1}.

4. CONCLUSIONS

According with our results the decrease on overpotential and the current increment for OER it is due to presences of Ru in the ternary material. $Pt_xRu_yIr_z$ synthesized by chemical reduction was unstable after subjected only to OER after several cycles. Different alloy phases were encountered in $Pt_xRu_yIr_z$ material after made the analysis with SEM and HRTEM, including Ruthenium phase and unidentified nanowires phase formation. Pt_xIr_z material was unstable material too; the current was decreasing as anodic potential applying was repeated.

Pt_xIr_z material showed an adequate material for ORR. There were no changes after several cycles. However the electrochemical activity of Pt_xIr_z was stable for ORR at different applied cycles, in contrast for $Pt_xRu_yIr_z$ the activity was improve after 100 cycles for the same reaction. The activity of content of Ruthenium phase in ternary material was a disadvantage by not activity after anodic potential.

ACKNOWLEDGEMENTS
This work was supported under the project PAPIT- IN18012, L. Morales S. would like to thank to Instituto de Energías Renovables for the facilities and logistic support and the CONACYT scholarship. The authors wish also to thank to José Chávez and Omar Novelo of IIM-UNAM for their assistance in TEM and EDS measurements. Maria Luisa Garcia and Rogelio Moran from IER-UNAM for their assistance in DRX and SEM analyses, and also Orlando Hernández of IF-UNAM for HRTEM measurements.

References

1. F. Mitlitsky, B. Myers, A.H. Weisberg, & T.M. Molter, *Fuel Cell Seminar*, Palm Springs CA, November(1998)16-19.
2. A.H. Weisberg, *Hydrogen Program Review-DOE*, VA April 28-30, 1998.
3. T. Ioroi, N. Kitazawa, K. Yasuda, Y. Yamamoto, & H. Takenaka, *J. of Applied Electrochemistry*, 31 (2001) 1179-1183.
4. T. Ioroi, T. Oku, K. Yasuda, N. Kumagai, Y. Miyazaki, *J Power Sources* 124 (2003) 385-389.
5. LL. Swette *J. Power Sources*, 47 (1994) 343-51.
6. Y. Zhang, C. Wang, N.Wan, Z. Mao. W. *International Journal of Hydrogen Energy*, 32 (2007) 400-404.
7. T. Ioroi, K. Yasuda, K. Siroma, N. Fujiwara, & Y. Miyazaki,. *Journal of Power Sources* 112 (2002) 583-587.
8. S. Altmann, T. Kaz, & K.A. Friedrich, *Electrochimica Acta*, 56 (2011) 4287-4293.
9. H. Y. B. Liu, *Electrochem. Solid State Lett*., 7(3) (2004) 56-9
10. G.Y. Chen, *Catalysis Today* 67 (2001) 341-355.
11. S. Sui, L. Ma, & Y. Zhai, *Journal of Power Sources*, 196 (2011) 5416-5422.
12. S.A. Grigoriev, P. Millet, K. Dzhus, H. Middleton, T.O. Saetre, & V.N. Fateev, *International Journal of Hydrogen Energy*, 35 (2010) 5070-5076.
13. H.Y. Jung, S. Park, & B.N. Popov, *Journal of Power Sources* 191 (2009) 357-361.
14. S.Y. Huang, P. Ganesan, H.Y. Jung, & B.N. Popov, *Journal of Power Sources*, 198 (2011) 23-29
15. F.D. Kong, S. Zhang, G.P. Yin, Z.B. Wang, C.Y. Du, G.Y. Chen, & N. Zhang, *International Journal of Hydrogen Energy* 37(2012)59-67.
16. J. Pettersson, B. Ramsey, & D. Harrison, *Journal of Power Sources*, 157(1) (2006). 28-34.
17. P. Sivakumar, & V. Tricoli, V. *Electrochemical and Solid-State Letters*, 9(3), (2006)A167.
18. S. Pasupathi, & V. Tricoli, *Journal of Solid State Electrochemistry*, 12(9) (2007)1093–1100.
19. Jingpeng Wang, Peter Holt-Hindle, Duncan MacDonald, Dan F. Thomas, Aicheng Chen. *Electrochimia Acta*, 53 (2008) 6944–6952.
20. A. Chen and Peter Holt-HindleChen, *Chem. Rev*. 110(2010)3767–804.
21. Y. Liang, H.Zhang, H. Zhong, X. Zhu, Z. Tian, D. Xu, D., & B. Yi, *J. Catal*. 238(2006) 468–476.
22. Y. Bo, L. Qingye, W. Yang, Z. Li, L. Juntao, and L. Peifang, *Catalysts. Chem. Mater*. 15(2003)3552-3557.
23. V. Radmilović, H.A. Gasteiger, P.N. Ross Jr. *J. Catal*., 154(1995)98.

24. Antolini, E.; Cardellini, F.; Giorgi, L.; Passalacqua, E. *J. Mater.Sci. Lett*. 19(2000) 2099.
25. Antolini, E.; Cardellini, F. *J. Alloys Compd*. 315(2001) 118.
26. X. Zhang and C. Kwong-Yu, *Chem. Mater*. 15(2003) 451-459.
27. J. C. Cruz, A. Ramos Hernández, M. Guerra-Balcazar, A.U. Chávez-Ramirez, J. Ledesma-García, L.G. Arriaga, *Int. J. Electrochem.Sci.*, 7(2012)7866-7876.
28. A.S. Aricó, P.L. Antonucci, E. Modica, V. Baglio, H. Kim, V, *Electrochimica Acta* 47(2002)3723-3732.
29. Eguiluz, K. I. B., Salazar-Banda, G. R., Miwa, D., Machado, S. a. S., & Avaca, L. A., *Journal of Power Sources* 179(2007) 42–49
30. William D. Callister and David G. Rethwisch, Materials Science and Engineering: An Introduction, Ed. Wiley, January 2010, ©2009
31. F. Liu, J.Y. Lee, W. Zhou, *Adv. Funct. Mater.*15(2005)1459.
32. J. Chen, T. Herricks and Y. Xia, Angew. *Chem., Int. Ed*.,44(2005)2589.
33. J. Chen, T. Herricks, M. Geissler and Y. Xia, *J. Am. Chem. Soc*.126(2004) 10854..
34. J. Chen, Y. Xiong, Y. Yin and Y. Xia, *Small,* 2(2006)1340.
35. L. Jorissen, J. Power Sources 155(2006) 23–32.,
36. J. Pettersson, B. Ramsey and D. J. Harrison, *Electron. Lett.*, 42(2006)1444-1446.
37. T. Loučka. *J Appl Electrochem* 7(1977)211.
38. R. Kotz and S. Stucki, *J Electroanal Chem* 172(1984) 41.
39. Reier, T., Oezaslan, M., & Strasser, P. *ACS Catalysis* 2(2012) 1765–1772
40. J. Bard and L.R. Faulkner, Electrochemical methods, fundamentals and applications. 2nd edition. John Willey &Sons, New York (2000).
41. A. Ezeta-Mejía, E.M.Arce Estrada, *Memorias del IX Congreso Internacional de la SMH*, Saltillo, México, 2009.
42. R. G. González-Huerta, J.A. Chávez-Carvayar and O. Solorza-Feria. *J. Power Sources*, 153(2006)11.
43. J.J. Salvador-Pascual, S. Citalàn-Cigarroa and O. Solorza-Feria, *J. Power Sources*,172(2007)229.
44. G. Ramos-Sànchez, H. Yee-Madeira and O. Solorza-Feria, *Int. J. Hydrogen Energy* 33(2008)3596.